Revision 1

Phase relationships in the system K_2CO_3-$CaCO_3$ at 6 GPa and 900-1450ºC

Anton Shatskiy[1,2*], Yuri M. Borzdov[1], Konstantin D. Litasov[1,2], Igor S. Sharygin[1,2], Yuri N. Palyanov[1,2], Eiji Ohtani[3]

[1]V.S. Sobolev Institute of Geology and Mineralogy, Russian Academy of Science, Siberian Branch, Koptyuga pr. 3, Novosibirsk 630090, Russia

[2]Novosibirsk State University, Pirogova Str. 2, Novosibirsk 630090, Russia

[3]Department of Earth and Planetary Material Science, Tohoku University, Sendai 980-8578, Japan

Abstract

Phase relations in the system K_2CO_3-$CaCO_3$ have been studied in the compositional range, $X(K_2CO_3)$, from 100 to 10 mol%, at 6.0 GPa and 900-1450 °C. At 900-950 °C the system has three intermediate compounds: $K_6Ca_2(CO_3)_5$, $K_2Ca(CO_3)_2$ and $K_2Ca_3(CO_3)_4$. The $K_2Ca(CO_3)_2$ compound decomposes to the $K_6Ca_2(CO_3)_5$ + $K_2Ca_3(CO_3)_4$ assembly above 950 °C. The $K_6Ca_2(CO_3)_5$ and $K_2Ca_3(CO_3)_4$ compounds melt congruently slightly above 1200 and 1300 °C, respectively. The eutectics were established at 64 and 44 mol% near 1200 °C and at 23 mol% near 1300 °C. K_2CO_3 remains as a liquidus phase at 1300 °C and 75 mol% and melts at 1425±20 °C. Aragonite remains as a liquidus phase at 1300 ºC and 20 mol% and at 1400 ºC and 10 mol% . $CaCO_3$ solubility in K_2CO_3 and K_2CO_3 solubility in aragonite are below the detection limit (<0.5 mol%).

Infiltration of subduction-derived K-rich Ca-Mg-Fe-carbonatite into the Fe^0-saturated mantle causes the extraction of $(Mg,Fe)CO_3$ components from the melt, which shifts its composition toward K-Ca-carbonatite. According to our data this melt can be stable at the *P-T* conditions of subcratonic lithosphere with geothermal gradient of 40 mW/m^2 corresponding to temperature of 1200 °C at 6 GPa.

Keywords: alkaline carbonates; buetschliite; fairchildite; high-pressure experiment; carbonatite; Earth's mantle.

Introduction

Carbonates are one of the important classes of compounds in the Earth's mantle which lower solidi of mantle rocks resulting in an appearance of carbonatite melt (Wyllie and Huang, 1975; Wallace and Green, 1988; Sweeney, 1994; Dalton and Presnall, 1998; Luth, 2006; Litasov, 2011). The latter is known as an effective metasomatic agent altering mantle geochemistry (Green and Wallace, 1988; Haggerty, 1989) and as a solvent-catalyst promoting crystallization of sublithospheric diamonds (Akaishi et al., 1990; Pal'yanov et al., 2002; Shatskii et al., 2002; Palyanov and Sokol, 2009). Besides, carbonates are important carbon carriers responsible for the carbon inflow into the mantle with subducting slabs and outflow with deep magmas (Dasgupta and Hirschmann, 2010; Dobretsov and Shatskiy, 2012).

The specific feature of deep carbonatite melts is high alkali contents (particularly K) as follows from studies of the melt inclusions in diamonds (Navon, 1991; Schrauder and Navon, 1994; Izraeli et al., 2004; Klein-BenDavid et al., 2004; Tomlinson et al., 2006; Weiss et al., 2009; Zedgenizov et al., 2009; Logvinova et al., 2011; Zedgenizov et al., 2011) and high-pressure experiments on partial melting of

carbonatites (Litasov et al., 2013), kimberlites (Litasov et al., 2010b; Sharygin et al., 2013), carbonated peridotites (Dasgupta and Hirschmann, 2007; Brey et al., 2011), eclogites (Dasgupta et al., 2004; Yaxley and Brey, 2004; Litasov et al., 2010a) and pelites (Grassi and Schmidt, 2011). Experimental data on synthesis of K-bearing clinopyroxene (Harlow, 1997) suggests that clinopyroxenes from inclusions in diamonds and diamond-bearing metamorphic rocks with up to 1 wt% K_2O (Sobolev et al., 1972; Sobolev and Shatsky, 1990; Harlow and Veblen, 1991; Sobolev et al., 1991; Shatsky et al., 1995) are crystallized from ultrapotassic carbonate-silicate melts containing 15–28 wt% K_2O.

It is thus essential to know phase relations in binary and more complex carbonate systems under mantle conditions. Since carbonates could participate in a variety of mantle processes (kimberlite magma generation, mantle metasomatism and diamond formation) which have been occurred at the base of subcratonic mantle (150-230 km depths), pressure of about 6 GPa is most interesting for the study of those systems. Although phase relations in the $CaCO_3$-$MgCO_3$ (Buob et al., 2006), $CaCO_3$-$FeCO_3$ (Shatskiy et al., 2014), K_2CO_3-$MgCO_3$ (Shatskiy et al., 2013c), Na_2CO_3-$MgCO_3$ (Shatskiy et al., 2013a) and Na_2CO_3-$CaCO_3$ (Shatskiy et al., 2013d) systems were already studied at 6 GPa, the data on phase relations in the K_2CO_3-$CaCO_3$ system are limited by pressures ≤ 0.1 GPa (Niggli, 1916; Eitel and Skaliks, 1929; Kröger et al., 1943; Ragone et al., 1966; Chattaraj et al., 1973; Cooper et al., 1975; Malik et al., 1985; McKie, 1990; Jago and Gittins, 1991; Arceo and Glasser, 1995) (Fig. 1). Therefore, in this paper we present experimental data on phase relations in the system K_2CO_3-$CaCO_3$ at 6 GPa and 900-1450ºC.

Experimental method

Experiments have been conducted using a pressless split-sphere apparatus "BARS" (Pal'yanov et al., 1997; Shatskiy et al., 2011a) equipped with an 8-6 type multianvil system at the V.S. Sobolev IGM SB RAS (Novosibirsk, Russia) (Palyanov et al., 2010) and a Kawai-type wedge and DIA uniaxial presses at Tohoku University (Sendai, Japan) (Lloyd et al., 1963; Osugi et al., 1964; Shatskiy et al., 2011b). BARS has been chosen due to its large sample volume ($V = 3.14 \times 5^2 \times 8 = 628$ mm^3) allowing loading over 40 1-mm samples in a single experiment and study phase relations in several carbonate systems simultaneously. The Kawai-type cell assembly with smaller sample volume ($V = 3.14 \times 2^2 \times 6 = 75$ mm^3) containing 16 samples have been employed to verify eutectic and melting temperatures depending on sample drying conditions.

In the BARS experiments, we employed a ZrO_2 pressure medium (PM) shaped as tetragonal prism (20.4×20.4×25.2 mm) and tubular graphite heater, 13/12 mm in outer/inner diameter and 19 mm length (Fig. 2). The PM was compressed by two anvils with 16×16 mm square and four anvils with 16×20 mm rectangular truncations. Temperature was monitored with a $Pt_{94}Rh_6/Pt_{70}Rh_{30}$ thermocouple calibrated at 5.7-6.3 GPa using the melting points of Al, Ag, Au, Ni, Pt, and Ni-C eutectic (Pal'yanov et al., 2002; Shatskii et al., 2002; Sokol et al., 2007). Pressure was calibrated by the graphite-diamond equilibrium in the Ni-C system (Kennedy and Kennedy, 1976) (Fig. 3, 4). The pressure and temperature were measured with the accuracy ±0.1 GPa and ±20 °C.

In the Kawai experiments, we used the ZrO_2 PM shaped as a 20.5-mm octahedron with ground edges and corners (see Fig. 1a in (Shatskiy et al., 2013c). Graphite heater, 4.5/4.0 mm in outer/inner diameter and 11 mm in length, was used to heat samples. The sample temperature was monitored using a $W_{97}Re_3/W_{75}Re_{25}$

thermocouple; no correction for the effect of pressure on thermocouple electromotive force was applied. The temperature was maintained within 0.5-2.0 °C of the desire value. Details of pressure calibration are given in figure 2 in (Shatskiy et al., 2013c). Deviation of pressure from the desirable value during heating to 900-1500 °C in the given cell and press load did not exceed ± 0.5 GPa, as confirmed by *in situ* X-ray diffraction experiments at the BL04B1 beamline of the SPring-8 synnhrotron radiation facility.

All experiments were performed using multiple graphite sample capsules (cassettes). No noble-metal outer capsule was used in our experiments. Because of its chemical inertness and high-melting point, graphite is preferable capsule material for the extremely mobile and reactive carbonate melts (Kanda et al., 1990; Shatskii et al., 2002). Besides, cheapness of graphite allows manufacturing thick-walled (≥ 0.4 mm in thickness) multi-sample holders, whereas its softness greatly facilitates the multi-charged assembly preparation, cutting and polishing recovered cassettes with samples.

Maximum radial and axial thermal gradients across the sample charges were examined using thermal modeling software (Hernlund et al. 2006) and were found to be 4 and 5 °C/mm in the BARS experiments and 5 and 10 °C/mm in the Kawai experiments (Fig. 3 in (Shatskiy et al., 2013c). Thus, the maximum temperature difference between samples did not exceed 20 °C.

We conducted two sets of experiments. In the first one, the samples in graphite cassettes were dried at 100ºC for 12 hours. These experiments were conducted using both BARS and Kawai-type apparatuses. In the second set of experiments conducted using the Kawai-type wedge uniaxial press, the samples were dried at 300 ºC for 3-5 hours and PM with other ceramic parts were fired at 950 ºC for 2 hours. Then assembly was stored at 130ºC for 6-12 hours in vacuum prior to experiment. During

opening the vacuum oven was filled with air from a drying oven rather than ambient air. Similar drying procedure allowed growth of nearly anhydrous (<68±4 wt ppm H_2O) Mg_2SiO_4 wadsleyite single crystals using $K_2Mg(CO_3)_2$ as a solvent (Shatskiy et al., 2009). Experimental conditions of the first and second sets of experiments are listed in Table 1 and 2, respectively.

The K_2CO_3-bearing samples are very hydroscopic and adsorb large amounts of water within minute under atmosphere conditions. Therefore, a special care was taken to minimize the time of contact between the samples and air. Recovered samples were mounted into an epoxy resin and polished in low-viscosity oil using 400-, 1000- and 1500-mesh sandpapers and 3-μm diamond paste. We used low-viscosity grade of epoxy, which can be drawn into pores and cracks by vacuum impregnation. The sample surface was cleaned using an oil spray between each step of polishing. The samples were always covered by a film of oil during polishing and checking up on the polishing progress under binocular microscope. Finally we used petroleum benzene to remove oil after polishing immediately prior to coating and loading the sample into a scanning electron microscope. Samples were studied using a JSM 5410 scanning electron microscope equipped with Oxford Instruments Link ISIS Series 300 energy-dispersive X-ray spectroscopic (EDS) microanalysis system at Tohoku University (Sendai, Japan). EDS spectra were collected by rastering the electron beam over a surface area available for the analysis with linear dimensions from 10 to 300 μm at 15 kV accelerating voltage and 1 nA load current. No beam damage or change in measured composition with time was observed at these settings. The correctness of the EDS measurements was confirmed under the same conditions using post-experimental samples with known compositions and homogeneous textures obtained below the solidus.

151

152 **Experimental results**

153 Representative BSE images of sample cross-sections are shown in Figures 5 and
154 6. The subsolidus samples were represented by homogeneous aggregates of carbonate
155 phases, with grain size varying from several tens to hundred micrometers. In non-
156 stoichiometric mixtures, the limiting reagents, i.e. K_2CO_3 at $X(K_2CO_3) < 60$ mol% and
157 $CaCO_3$ at $X(K_2CO_3) > 25$ mol% have been consumed completely (Table 1, 2). In
158 stoichiometric mixture, $X(K_2CO_3) = 60$ mol% both reagents, K_2CO_3 and $CaCO_3$, were
159 completely consumed to form the $K_6Ca_2(CO_3)_5$ compound (Table 1, 2). This suggests
160 that reactions have gone to completion and equilibrium has been achieved.

161 An aggregate of carbonate crystals up to 200 μm in size in the cool region and
162 a quenched melt segregated to the hot region of the sample capsule were observed in
163 the run products below the liquidus (Fig. 5 and 6). The melts quenched with a rate of
164 about 60°C/sec, were represented by dendritic aggregates. Extensive quench
165 crystallization is common feature of the carbonate and carbonate-silicate melts
166 (Ragone et al., 1966; Eggler, 1975; Buob et al., 2006; Keshav and Gudfinnsson, 2013),
167 which is attributed to their low viscosity (Dobson et al., 1996; Guillot and Sator,
168 2011) and high component diffusivities (Genge et al., 1995; Shatskiy et al., 2013b).
169 The liquid-crystal interface outlines (Fig. 5 and 6) coincide with the typical shape
170 expected for an isotherm in a high-pressure cell (see Fig. 2 in this manuscript and Fig.
171 3b in (Shatskiy et al., 2013c). For example, in the BARS experiments, the melt
172 segregates from the heater side (Fig. 5f,h) in samples from the middle cassette (Fig. 2).
173 In the Kawai experiments, the melt segregates at the sample ends (Fig. 6e,k,o) located
174 at the heater center. In all cases the melt segregates in the high-temperature region
175 independently from the gravity vector. The cause of liquid and solid phases

redistribution in the thermal gradient field and formation of the rounded interface has been discussed in our previous study (Shatskiy et al., 2010).

Alkali-carbonate melts are known as very mobile and extremely reactive compounds, which are difficult to seal in a high-pressure cell. To overcome this encapsulation problem we used tightly closed graphite capsules (Fig. 2). Since our multicharge experiments also contained carbonate samples with different cation compositions such as Na-Ca, Na-Mg, or K-Mg, which in some cases were loaded into the same cassette, it was easy to monitor the performance of those capsules at given *P-T* conditions and run durations in terms of proper carbonate melt sealing. EDS analysis did not show any foreign cations in our post-experimental samples.

Both K_2CO_3 and $CaCO_3$ melts are known as solvent catalysts for the graphite-to-diamond transformation (Akaishi et al., 1990; Pal'yanov et al., 1998; Pal'yanov et al., 1999; Shatskii et al., 2002). Although our experiments were performed in the field of thermodynamic stability of diamond (Kennedy and Kennedy, 1976), no diamonds were found in the run products even after sample annealing at 1400 ºC and 6 GPa for 6 hours. This is consistent with previous results for the system K_2CO_3-C, in which no diamonds appeared even after 40 hours at 5.7 GPa and 1420 °C (Pal'yanov et al., 2002), while diamond nucleation was established at 6.3 GPa, 1650 °C with the same run duration (Shatskii et al., 2002). This can be explained by the long time required for diamond to nucleate in the carbonate systems, which diminishes with increasing temperature and pressure from ≥40 hours at 5.7 GPa and 1420 ºC to 20 minutes at 7 GPa and 1700-1750 ºC (Pal'yanov et al., 1999).

Experiments under "wet" conditions. Phase relations established in the first set of experiments with samples dried at 100 °C are illustrated in Fig. 7a. At 900 °C, the system has three intermediate compounds: $K_6Ca_2(CO_3)_5$, $K_2Ca(CO_3)_2$ and

$K_2Ca_3(CO_3)_4$. The second compound undergoes subsolidus breakdown above 900 °C according to the reaction: $7K_2Ca(CO_3)_2 = 2K_6Ca_2(CO_3)_5 + K_2Ca_3(CO_3)_4$. The distinct liquid compositions at 1100 ºC below and above 60 mol% K_2CO_3 and at 1150 °C below and above 25 mol% K_2CO_3 suggest a eutectic type phase diagram (Table 1, Fig. 7a). This is also supported by a coexistence of liquid with two solid phases in near eutectic compositions at 50 mol% K_2CO_3 and 1000 ºC (Fig. 5f). The topology of the phase diagram implies congruent melting of $K_6Ca_2(CO_3)_5$ above 1100 ºC and $K_2Ca_3(CO_3)_4$ above 1150 ºC (Fig. 7a). The eutectics were established at $X(K_2CO_3)$ = 66 mol% between 1000 and 1100 °C, at 46 mol% near 1000 °C and at 23 mol% near 1150 °C (Fig. 7a). The carbonate K_2CO_3 does not melt up to 1200 ºC, while complete melting was established at 1300 °C and $X(K_2CO_3)$ = 90 mol% (Table 1). Measurable amounts of $CaCO_3$ in K_2CO_3 suggest an existence of limited solid solutions of $CaCO_3$ in K_2CO_3 at given experimental conditions (Fig. 5a, b, Table 1). The maximum $CaCO_3$ solubility in K_2CO_3 of about 20 mol% was established at 1000 ºC (Fig. 7a). $CaCO_3$ was observed as a subliquidus phase at $X(K_2CO_3)$ = 20 mol% and 1150 ºC and at $X(K_2CO_3)$ = 10 mol% up to 1300 ºC. The K solubility in aragonite does not exceed the detection limit of EDS employed in our study (i.e. ≤ 0.5 mol% K_2CO_3) (Table 1).

Experiments under "dry" conditions. Phase relations established in the second set of experiments with samples dried at 300 °C are illustrated in Fig. 7b. At 1150 °C, the system has two intermediate compounds: $K_6Ca_2(CO_3)_5$ and $K_2Ca_3(CO_3)_4$. At $X(K_2CO_3)$ = 60 mol%, most of the sample consists of the $K_6Ca_2(CO_3)_5$ compound, and minor amount of quenched melt at the high-temperature sample end (Fig. 6f). The melt composition coincides (within measurement error of melt composition) with the composition of starting mixture and solid phase (Table 2). The same composition of solid and liquid phases suggests congruent melting of $K_6Ca_2(CO_3)_5$. The simultaneous

226 occurrence of solid and liquid phase is due to the axial thermal gradient along the
227 sample charge. At 1300 °C and $X(K_2CO_3)$ = 30 mol%, the $K_2Ca_3(CO_3)_4$ compound
228 coexists with melt containing 33 mol% K_2CO_3, whereas at $X(K_2CO_3)$ = 20 and 10
229 mol% aragonite coexists with melt containing 22 mol% K_2CO_3. This indicates
230 congruent melting of $K_2Ca_3(CO_3)_4$, which occurs between 1300 and 1400 °C (Fig. 7b).
231 Similar to the first set of experiments, the distinct liquid compositions at 1200
232 ºC and $X(K_2CO_3)$ below and above 60 mol% and at 1300 °C below and above 25
233 mol% suggest a eutectic type phase diagram (Table 2, Fig. 7b). The eutectics were
234 established at $X(K_2CO_3)$ = 63 mol% between 1150 and 1200 °C, at 44 mol% near
235 1200 °C and at 23 mol% near 1300 °C (Fig. 7b). The liquidus lines were drown based
236 on the melt compositions measured by EDS (Fig. 7b). As shown in Table 1, K_2CO_3
237 does not melt up to 1400 °C. Melting of K_2CO_3 was established in additional run in
238 the pure K_2CO_3 system at 1450 °C. $CaCO_3$, whose melting temperature is about 1680
239 ºC at 6 GPa (Suito et al., 2001; Shatskiy et al., 2014), was observed as a subliquidus
240 phase at $X(K_2CO_3)$ = 20 mol% and 1300 ºC and at $X(K_2CO_3)$ = 10 mol% and 1400 ºC.
241 It was identified by the Raman spectroscopy as aragonite.
242
243 **Discussion**
244 The results clearly demonstrate that insufficient sample drying significantly (by
245 about 200 ºC) lowers eutectic temperatures and widen the field of the K_2CO_3 solid
246 solutions (Fig. 7). At the same time the drying conditions have no significant effect on
247 the eutectic compositions. A gas chromatography measurements of recovered samples
248 from high-pressure experiments in sealed capsules show that water is a major volatile
249 in quenched carbonate melts (Sokol et al., 2000). Sokol et al. have concluded that
250 most of water detected in their samples was trapped during sample storage at 90 °C in

the oven. The water absorption during carbonate powder loading into the capsules without subsequent drying is another possible reason for sample hydration (Shatskiy et al., 2009). The latter possibility is also suggested by significant variations in the water contents in the recovered samples (from 0 to 0.45 wt% H_2O) reported by Sokol et al. (2000). In the second set of experiments we employed the drying procedure similar to that we used for growth of nearly anhydrous (<68±4 wt ppm H_2O) Mg_2SiO_4 wadsleyite single crystals from $K_2Mg(CO_3)_2$ melt (Shatskiy et al., 2009). Therefore, we assume that starting materials in the first set of experiments were contaminated by water, i.e., conducted under wet conditions, whereas the second one was conducted under nominally dry conditions. The water contamination can be associated with the formation of $K_2CO_3 \cdot 1.5H_2O$, which is almost impossible to prevent in air (Schneide and Levin, 1973; Deshpande et al., 1993).

The established melting temperature of K_2CO_3 at 6 GPa is about 250 °C higher than that at 3.2 GPa reported by (Liu et al., 2006). According to their data a slope (dT/dP) of the K_2CO_3 fusion curve decreases with pressure and begins to flatten at ~ 2.5 GPa (Fig. 8). At this pressure the density of the melt should be similar to that of the solid phase. In contrast, our data suggest a sharp increase in the dT/dP slope at higher pressures. This might occur due to a pressure-induced phase transition in solid K_2CO_3 (Cancarevic et al., 2006).

The stoichiometry of subliquidus K-Ca carbonates established at 6 GPa differs from that at 1 bar and 0.1 GPa pressures (Cooper et al., 1975; Arceo and Glasser, 1995) (Fig. 1 and 7). At 6 GPa, the "low-pressure" $K_2Ca(CO_3)_2$ compound (Cooper et al., 1975) appears only at 900°C under "wet" conditions (Fig. 7a), whereas at higher temperatures it is replaced by the $K_6Ca_2(CO_3)_5$ + $K_2Ca_3(CO_3)_4$ assemblage (Fig. 7). We also did not observed the $K_2Ca_2(CO_3)_3$ and $K_4Ca_5(CO_3)_7$ compounds which were

established at ambient pressure (Fig. 1 and 7). A comparison of the 6.0 GPa and 0.1 GPa data shows a significant increase in the eutectic temperatures with pressure: by about 400°C for the K-rich side and by ~500°C for the Ca-rich side of the K_2CO_3-$CaCO_3$ join (Fig. 1 and 7b).

The high eutectic temperature of $K_2Ca_3(CO_3)_4$ + aragonite assemblage (near 1300 °C at 6 GPa) suggests that the $K_2Ca_3(CO_3)_4$ compound can be one of the potential host of potassium at the *P-T* conditions of subcratonic lithosphere. The binary carbonate with similar stoichiometry, $Na_2Ca_3(CO_3)_4$, was also established in the Na_2CO_3-$CaCO_3$ system at 900-1300 °C and 6 GPa (Shatskiy et al., 2013d).

Since carbonate would be the major contributors to the incipient melting in the oxidized mantle domains under anhydrous conditions, it is interesting to compare phase relations in the Na/K_2CO_3-Ca/$MgCO_3$ binary diagrams at 6 GPa (Fig. 9). All these systems contain intermediate compounds, which melt congruently. The Na/K_2CO_3-$MgCO_3$ systems have one intermediate compound (Fig. 9a,b), whereas the Na/K_2CO_3-$CaCO_3$ systems have two intermediate compounds, which melt congruently and one compound, which decomposes under subsolidus conditions (Fig. 9c,d). In contrast to K_2CO_3, the solid Na_2CO_3 dissolve measurable amount of $MgCO_3$ (up to 9 mol%) and $CaCO_3$ (up to 8 mol%). The lowest temperature eutectics occur near 1200 °C on the alkali-rich side of these binary systems. The highest melting eutectics locate near 1250 °C on the Mg-rich side and near 1300 °C on the Ca-rich side of the corresponding binary systems (Fig. 9).

Compared with the eutectics determined in the binary carbonate systems, the solidi of K-bearing carbonated peridotite, $T_{Solodus} \leq 1100$ °C at 6 GPa (Brey et al., 2011), and K-bearing carbonated pelite, $T_{Solodus} \sim 1070$ °C near 6 GPa (Grassi and

Schmidt, 2011), are at lower temperatures. This difference undoubtedly reflects the influence of additional constituents, such as $MgCO_3$.

Implications for interaction of subduction-derived carbonatite melt with Fe^0-saturated mantle

Volatiles (H_2O and CO_2) are recycled back into the Earth's interior in the subduction zones. Thermodynamic modeling suggests that significant portion of carbonates stored in the sediment and basaltic layers can survive melting and devolatilization under the island arcs and be preferentially transported to the deep mantle, in contrast to H_2O and hydrous minerals (Kerrick and Connolly, 2001a; b). As subducting slabs sink to 200-300 km depths and warm up to 1100 °C sediments (carbonated pelites) undergo partial melting and yield potassic ankerite-dolomite melt $37(K_{\leq 0.94}Na_{\geq 0.06})_2CO_3 \cdot 63(Ca_{0.62}Mg_{0.16}Fe_{0.22})CO_3$ (0.6 мол% SiO_2) (Grassi and Schmidt, 2011). Owing to its low density (Genge et al., 1995; Guillot and Sator, 2011), enhanced wetting properties (Hunter and McKenzie, 1989; Minarik and Watson, 1995; Yoshino et al., 2010), and ability to transport silicate components (Shatskiy et al., 2013b), the carbonate melt can stem from subducted oceanic lithosphere and percolate upwards along grain boundaries (Hammouda and Laporte, 2000).

In contrast to oxidized subduction zones, the redox conditions in the lowermost upper mantle and transition zone may be controlled by presence of ~0.1 wt% Fe^0 which forms as a result of disproportionation reaction Fe^{2+} (olivine) = Fe^0 (metal) + Fe^{3+} (garnet) at pressures > 7 GPa (Rohrbach et al., 2007; Frost and McCammon, 2008). Therefore, subduction-derived carbonate melt must be partially reduced by metallic iron. Recent experimental study by Palyanov et al. (2013) shows that the

redox reaction, $CaCO_3 \cdot MgCO_3 \cdot FeCO_3$ (melt) + $4Fe^0$ (metal) = $CaCO_3$ (melt) + $MgO \cdot 5FeO$ (magnesiowustite) + 2C(diamond), causes the extraction of $(Mg,Fe)CO_3$ components from the melt and shifts the melt composition to essentially calcitic (Palyanov et al., 2013). The phase relations in the $CaCO_3$-$MgCO_3$-$FeCO_3$ system (Shatskiy et al., 2014) suggest that such change in the melt composition should cause its freezing and crystallization of Mg- and Fe-bearing calcite at temperature conditions of average mantle geotherm. In contrast, the partial reduction of the potassic ankerite-dolomite melt established by Grassi and Schmidt (2011) should shift its composition toward K-Ca carbonate melt. According to our data this melt can be stable at the *P-T* conditions of subcratonic lithosphere with geothermal gradient of 40 mW/m^2 corresponding to temperature of 1200 °C at 6 GPa (Pollack and Chapman, 1977; McKenzie et al., 2005).

Acknowledgements

We are very grateful to Dionysis Foustoukos and Shantanu Keshav for thorough review and Keith Putirka and Bjorn Mysen for editorial handling and personal attention. Special thanks to Robert Luth for the time he spent reviewing early versions of the manuscript, for his helpful suggestions and comments. This work was supported by the Russian Scientific Fund (proposal No. 14-17-00609) and performed under the project of the Ministry of education and science of Russian Federation (No. 14.B25.31.0032).

Table 1. Compositions (in mol% K_2CO_3) of the run products in the system K_2CO_3-$CaCO_3$ at 6 GPa under hydrous conditions.

Run No., *T*, time	Run products	*X*(K_2CO_3) in the system, mol% 90	75	60	55	50	40	30	20	10
B1487/2	K_2CO_3	–	–	–	–	–	–	–	–	–
1300ºC	Aragonite	–	–	–	–	–	–	–	×	0.4
2 h	Liquid	89.8(2.2)	+	+	+	50.3	39.6	29.7	×	13.2
B1488/2	K_2CO_3	97.6(1.0)	–	–	–	–	–	–	×	–
1200ºC	Aragonite	–	–	–	–	–	–	–	×	0.5
10 h	Liquid	85.0(1.5)	+	+	54.4(3)	49.2	41.8(4)	30.0(2)	×	16.6(6)
T2018	K_2CO_3	92.3(3)	91.8	–	×	–	–	–	–	–
1150ºC	$K_6Ca_2(CO_3)_5$	–	–	–	×	–	–	–	–	–
14 h	$K_2Ca_3(CO_3)_4$	–	–	–	×	–	24.5	25.0	24.7	24.6
	Aragonite	–	–	–	×	–	–	–	0.2(2)	0.3(0)
	Liquid	70.6(2)	67.5(2.4)	61.0(5)	×	+	+	+	21.7(2)	+
T2019	K_2CO_3	85.4(1.3)	86.2	–	×	–	–	–	–	–
1100ºC	$K_6Ca_2(CO_3)_5$	–	59.7	60.3(2)	×	59.0(3)	–	–	–	–
15 h	$K_2Ca_3(CO_3)_4$	–	–	–	×	–	25.2	25.0	24.4	24.1
	Aragonite	–	–	–	×	–	–	0.4	0.1	0.5
	Liquid	–	67.7	62.1(2)	×	52.1(9)	44.6(2)	43.9	–	–
ES335	K_2CO_3	×	×	–	×	–	–	–	–	–
1050ºC	$K_6Ca_2(CO_3)_5$	×	×	59.5(2)	×	58.6	–	–	–	–
19 h	$K_2Ca_3(CO_3)_4$	×	×	–	×	25.0(4)	24.9(4)	24.8(3)	24.5	24.5
	Aragonite	×	×	–	×	–	–	–	0.3(2)	0.1
	Liquid	×	×	–	×	48.0(2)	45.1(8)	44.3(3)	–	–
B1002/1	K_2CO_3	90.0(1.6)	80.5(6)	×	–	–	–	–	×	–
1000ºC	$K_6Ca_2(CO_3)_5$	–	60.4(2.9)	×	58.1(7)	59.8(2)	58.5(2)	59.6(4)	×	–
30 h	$K_2Ca_3(CO_3)_4$	–	–	×	25.2(0)	25.8	25.1(1.2)	24.6(0)	×	24.1
	Aragonite	–	–	×	–	–	–	–	×	0.4(2)
	Liquid	–	–	×	49.3(1)	45.9(7)	46.4(1.6)	46.4(5)	×	–
T2011	$K_2Ca(CO_3)_2$	×	×	×	×	×	51.2	×	–	–
950ºC	$K_2Ca_3(CO_3)_4$	×	×	×	×	×	26.1	×	26.0	25.1
36 h	Aragonite	×	×	×	×	×	–	×	0.5(2)	0.4(2)
B1000/1	K_2CO_3	92.7(5)	91.9	×	–	–	–	–	×	–
900ºC	$K_6Ca_2(CO_3)_5$	59.8(1.5)	58.5	60.1(3)	59.1	–	–	–	×	–
38 h	$K_2Ca(CO_3)_2$	–	–	×	50.3(1)	50.0(5)	50.3(7)	50.3(3)	×	–
	$K_2Ca_3(CO_3)_4$	–	–	×	–	–	24.5	24.9(1.7)	×	25.5
	Aragonite	–	–	×	–	–	–	–	×	0.0

Notes: "–" – phase was not established in the run products; "+" – complete melting; × – no data. Standard deviations are given in parentheses, where the number of measurements is more than one. Letters in the run number, denote the type of multianvil apparatus, ES = wedge, T = DIA and B = BARS.

Table 2. Compositions (in mol% K_2CO_3) of the run products in the system K_2CO_3-$CaCO_3$ at 6 GPa under nominally dry conditions.

Run No., T, time	Run products	$X(K_2CO_3)$ in the system, mol% 90	75	60	50	40	30	20	10
ES346	K_2CO_3	100.0[A]	×	×	×	×	–	–	–
1400ºC	Aragonite	–	×	×	×	×	–	–	0.2
6h	Liquid	–	×	×	×	×	31.0	+	12.9(2)
ES344	K_2CO_3	99.9	100.0	–	–	–	–	–	–
1300ºC	$K_6Ca_2(CO_3)_5$	–	–	–	–	–	–	–	–
4h	$K_2Ca_3(CO_3)_4$	–	–	–	–	–	25.7	–	25.4
	Aragonite	–	–	–	–	–	–	0.1	0.4(3)
	Liquid	71.1	70.6(1)	60.2(1)	49.2(2)	40.0(3)	32.6(4)	22.1(2)	22.2
ES341	K_2CO_3	99.3	100.0	–	–	–	–	–	–
1200ºC	$K_6Ca_2(CO_3)_5$	61.0	59.2	59.7	57.9	–	–	–	–
12h	$K_2Ca_3(CO_3)_4$	–	–	–	25.3	25.4	25.0	24.5	23.1
	Aragonite	–	–	–	–	–	–	0.2	0.4(1)
	Liquid	+	65.1(6)	61.9	45.2	44.1(6)	44.5(4)	–	–
ES347	K_2CO_3	99.2	99.1	–	–	–	–	–	–
1150ºC	$K_6Ca_2(CO_3)_5$	60.1	61.3	59.5	60.3	60.3	59.1	–	–
18 h	$K_2Ca_3(CO_3)_4$	–	–	–	25.6(2.4)	25.0	24.9	24.6	24.2
	Aragonite	–	–	–	–	–	–	0.3	0.4

Notes: "–" – phase was not established in the run products; "+" – complete melting; × – no data. Standard deviations are given in parentheses, where the number of measurements is more than one. Letters in the run number, "ES" denotes the uniaxial press with wedge-type guide-block. [A] – The pure K_2CO_3 system.

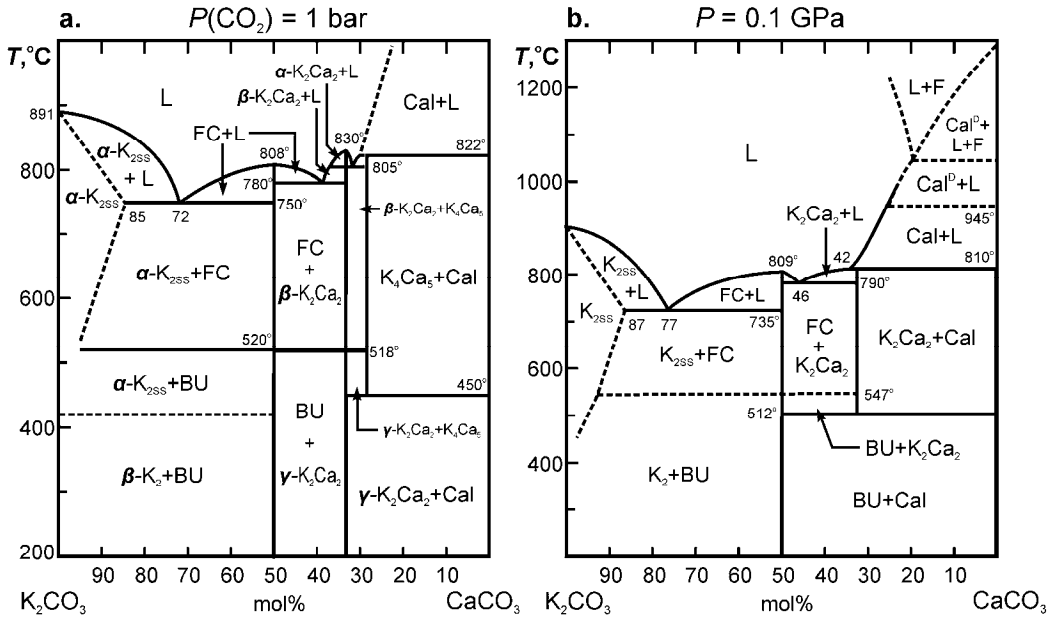

Fig. 1. Phase relations in the system K_2CO_3-$CaCO_3$ at 1 bar CO_2 pressure (Arceo and Glasser, 1995) (a) and at pressure of 0.1 GPa (Cooper et al., 1975) (b). K_2 – K_2CO_3; K_{2SS} – $CaCO_3$ solid solution in K_2CO_3; BU – buetschliite, $K_2Ca(CO_3)_2$; FC – fairchildite, $K_2Ca(CO_3)_2$; K_2Ca_2 – $K_2Ca_2(CO_3)_3$; K_4Ca_5 – $K_4Ca_5(CO_3)_7$; Cal – calcite; Cal^D – disordered calcite; L = liquid; F = CO_2 fluid.

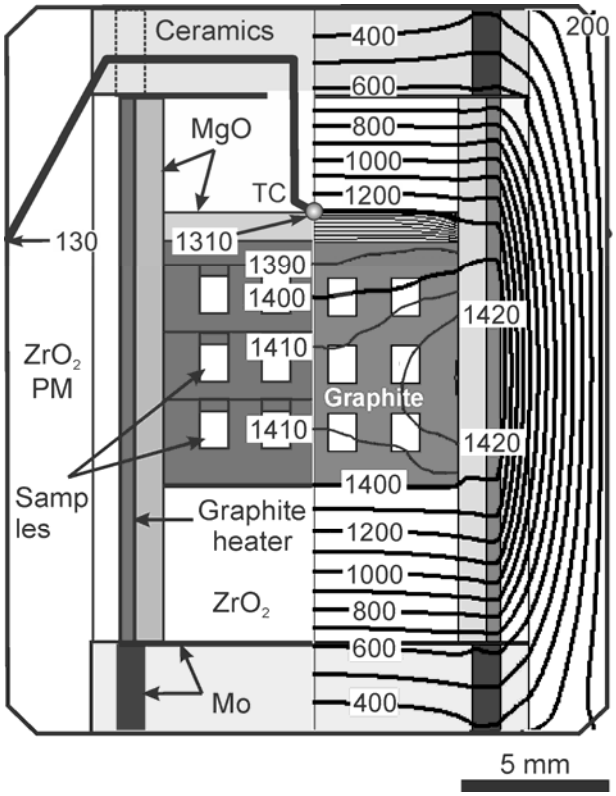

Fig. 2. High-pressure cell assembly employed to study phase relations in carbonate systems at 6 GPa using pressless split-sphere apparatus (BARS) (Palyanov et al., 2010). The temperature distribution along the cell obtained using the thermal modeling software (Hernlund et al., 2006) is given at the right side of the figure in °C. TC – PtRh(30/6) thermocouple; PM – pressure medium.

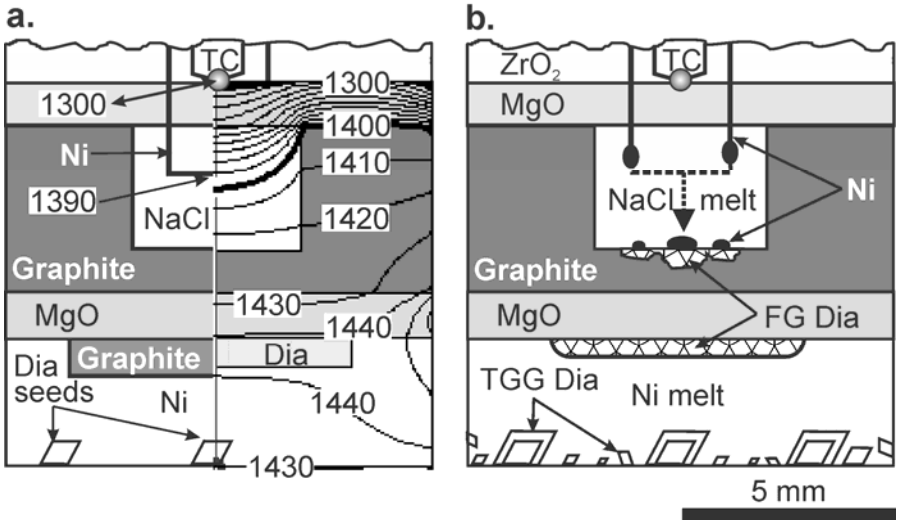

374

375 Fig. 3. An assembly design in the calibration experiments for BARS. (a) The
376 sample chamber arrangement and temperature distribution are shown in °C. (b)
377 Scheme of Ni melting and diamond crystallization. Dia – diamond; FG – film growth;
378 TGG – thermal gradient growth; TC – PtRh(30/6) thermocouple junction. Melting
379 point of the metal wire was detected by resistance jump.

380

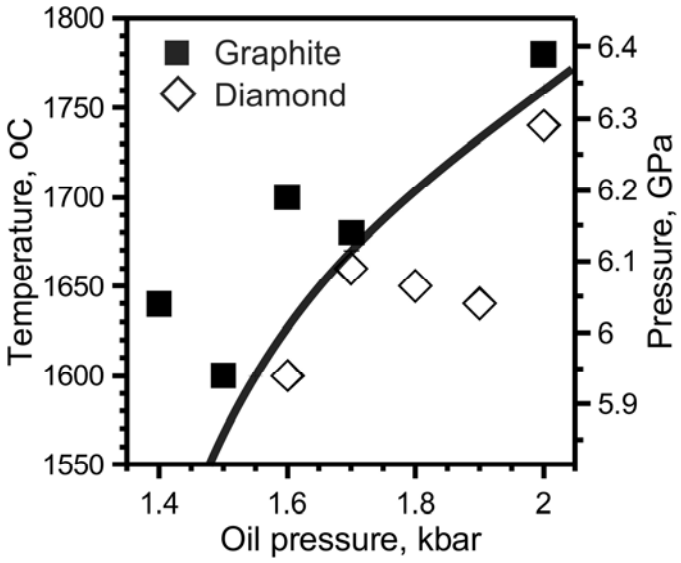

Fig. 4. Pressure calibration of a 8-6 type multianvil system with TEL 16 and 20 mm and ZrO_2 PM shaped as tetragonal prism (20.4×20.4×25.2 mm). We placed composite metal gaskets between anvils near truncations to minimize extrusion of the PM and to improve stress distribution inside anvils (Shatskiy et al., 2011; Yoneda et al., 1984).

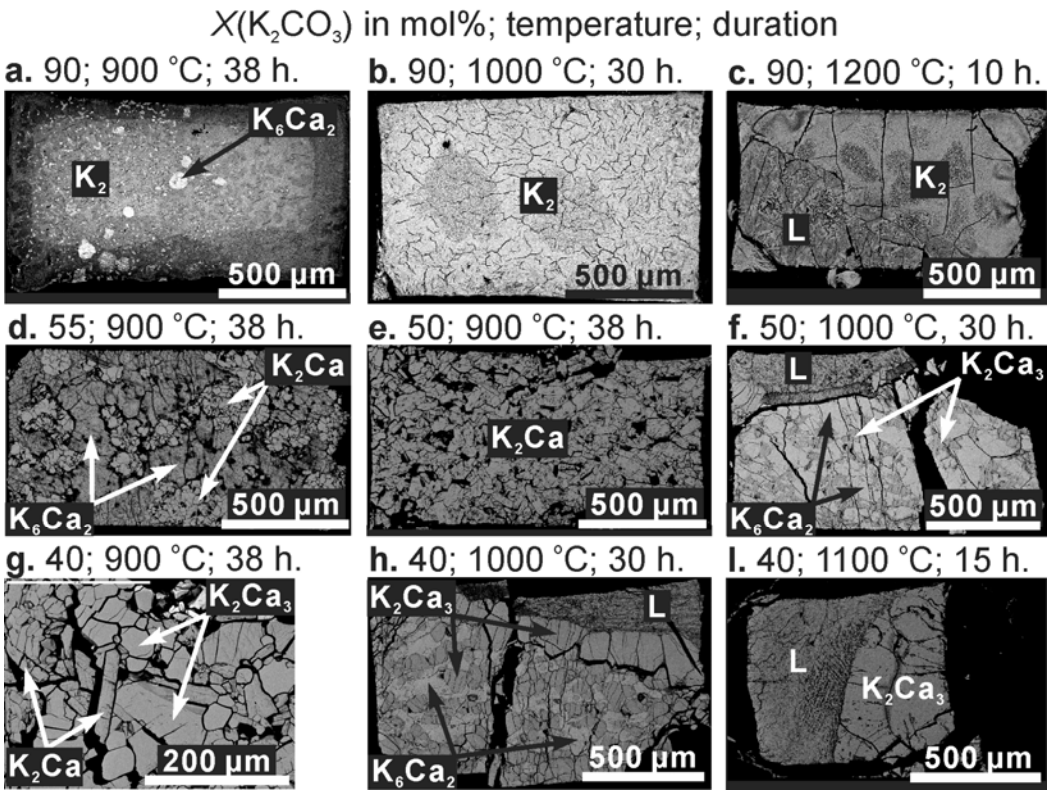

Fig. 5. Representative BSE images of sample cross-sections illustrating phase relations in the system K_2CO_3-$CaCO_3$ at 6 GPa under "wet" conditions (i.e. in samples dried at 100 °C). Sample axes are horizontally disposed on each image. In the experiments, the sample exes were disposed vertically. Melt always segregates in high-temperature region independently of gravity. K_2 = K_2CO_3 solid solution; K_6Ca_2 = $K_6Ca_2(CO_3)_5$; K_2Ca = $K_2Ca(CO_3)_2$; K_2Ca_3 = $K_2Ca_3(CO_3)_4$; L = liquid.

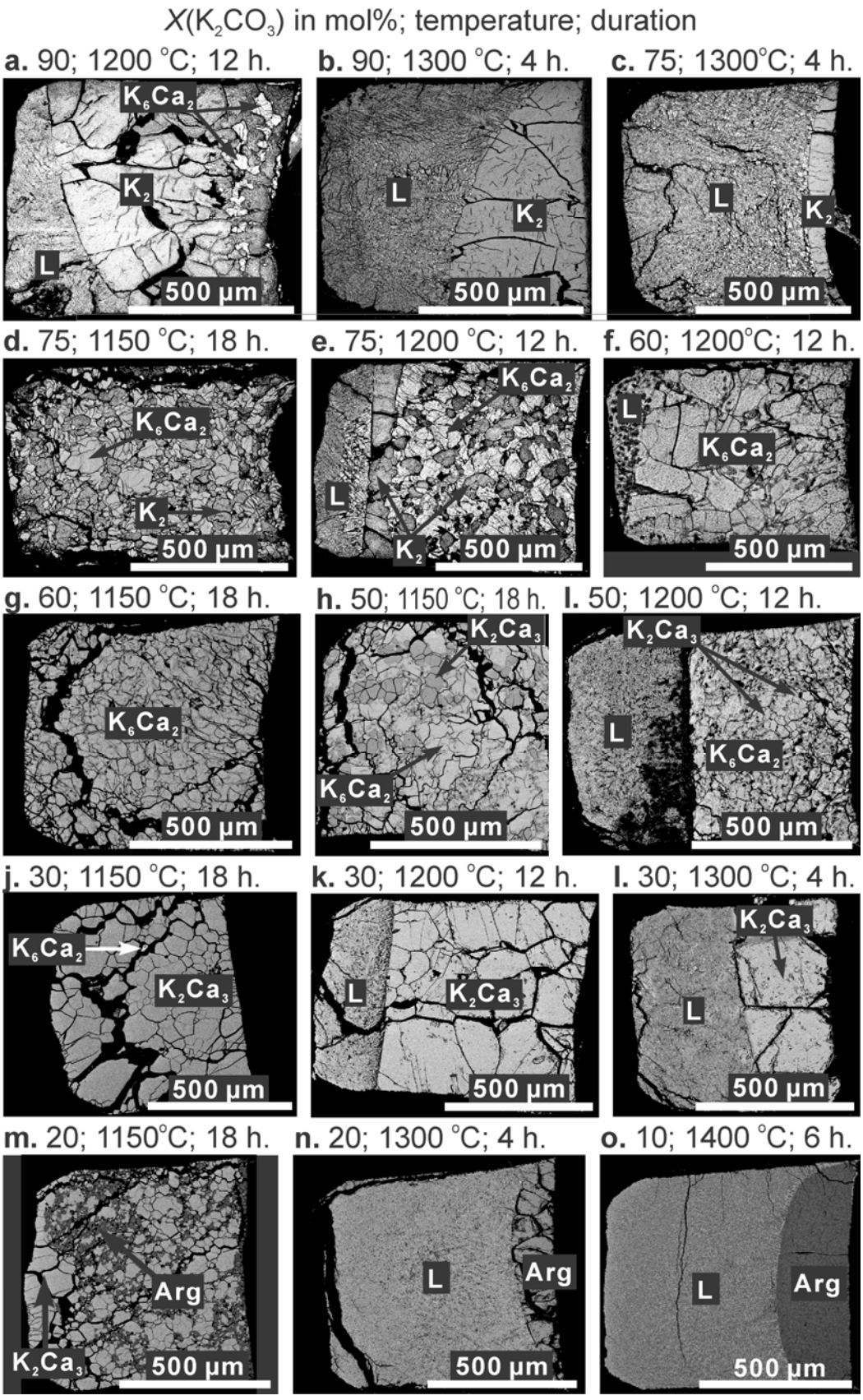

398

399 Fig. 6. Representative BSE images of sample cross-sections illustrating phase
400 relations in the system K_2CO_3-$CaCO_3$ at 6 GPa under nominally "dry" conditions (i.e.
401 in samples dried at 300 °C). Sample axes are horizontally disposed on each image. In
402 the experiments, the sample axes were tilted by 54.7º. The upper sample end is
403 located on the right side of each image. Melt always segregates in high-temperature
404 region independently of gravity. K_2 = K_2CO_3; K_6Ca_2 = $K_6Ca_2(CO_3)_5$; K_2Ca_3 =
405 $K_2Ca_3(CO_3)_4$; Arg = aragonite; L = liquid.
406

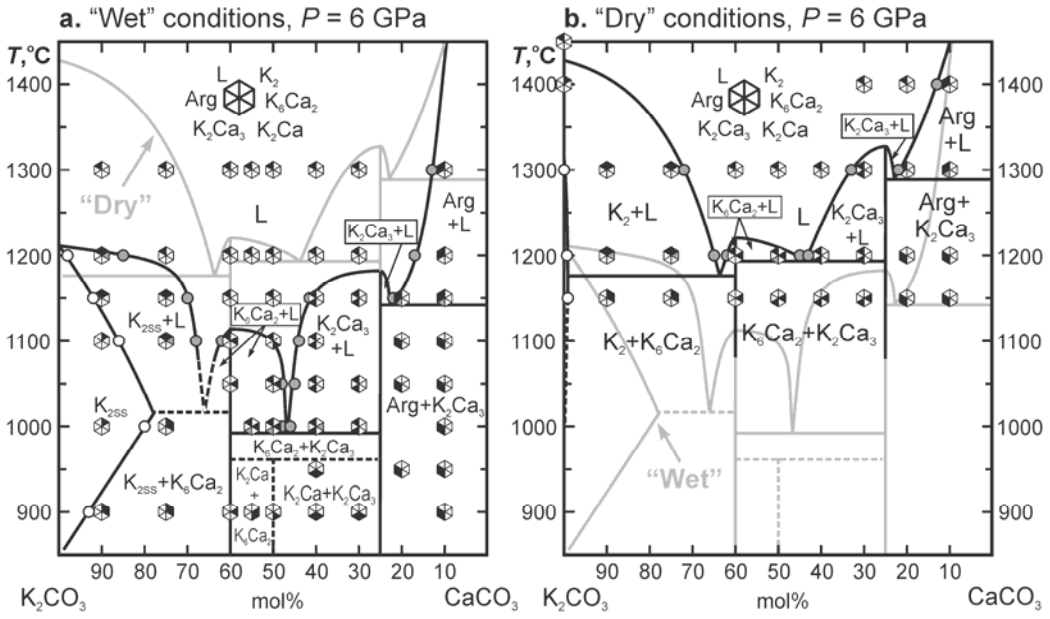

407

408 Fig. 7. Phase relations in K_2CO_3-$CaCO_3$ system at 6 GPa under "wet" and "dry"
409 conditions, i.e. in samples dried at 100 and 300 °C, respectively. K_2 = K_2CO_3; K_{2SS} =
410 $CaCO_3$ solid-solution in K_2CO_3; K_6Ca_2 = $K_6Ca_2(CO_3)_5$; K_2Ca = $K_2Ca(CO_3)_2$; K_2Ca_3 =
411 $K_2Ca_3(CO_3)_4$; Arg = aragonite; L = liquid. Grey circles indicate the melt composition
412 measured by EDS. White circles mark the composition of $CaCO_3$-K_2CO_3 solid
413 solution. Grey segments in hexagons denote phases observed at the lower temperature
414 side of the samples.

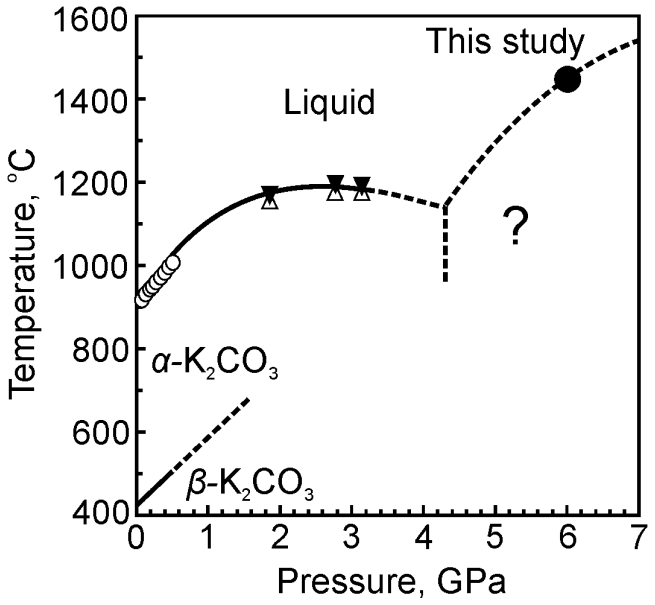

Fig. 8. The K_2CO_3 fusion curve. The open circles are the experimentally determined melting temperatures from (Klement and Cohen, 1975). The open and filled triangles are the experimentally determined melting temperatures from (Liu et al., 2006). β-K_2CO_3 is monoclinic, $C2/c$, and α-K_2CO_3 is hexagonal, $P6_3/mmc$, K_2CO_3 polimorphs (Schneide and Levin, 1973; Becht and Struikmans, 1976; Dinnebier et al., 2005). The α-β transition slope was experimentally determined up to 0.5 GPa (Klement and Cohen, 1975).

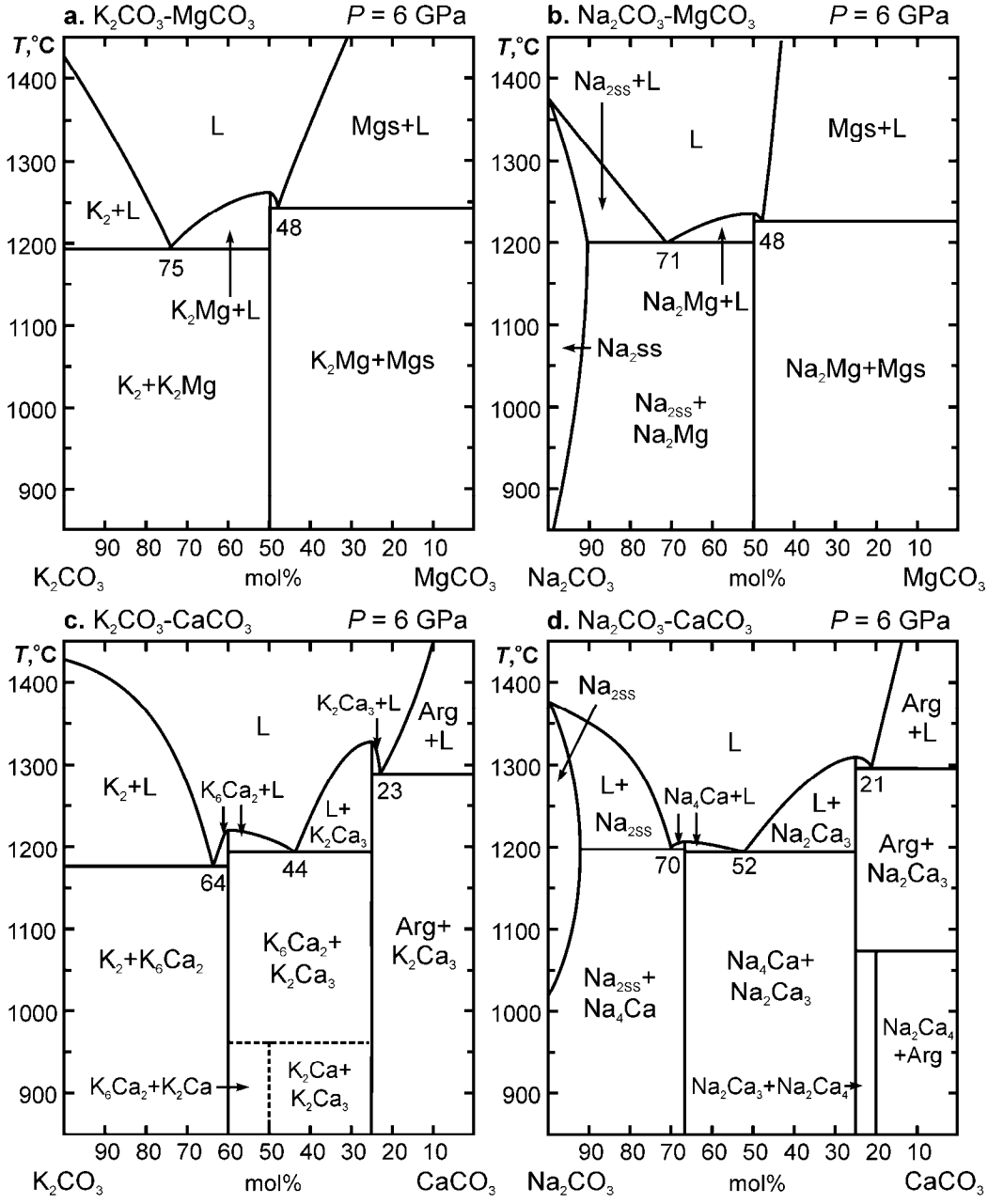

Fig. 9. Comparison of phase relations in the binary alkali-alkaline earth carbonate systems at pressure of 6 GPa. (a) The system K_2CO_3-$MgCO_3$ (Shatskiy et al., 2013c). (b) The system Na_2CO_3-$MgCO_3$ (Shatskiy et al., 2013a). (c) The system K_2CO_3-$CaCO_3$ (this study). (d) The system Na_2CO_3-$CaCO_3$ (Shatskiy et al., 2013d). Numbers indicate mole fraction of alkaline component at the eutectic points.

References cited

Akaishi, M., Kanda, H., and Yamaoka, S. (1990) Synthesis of diamond from graphite-carbonate systems under very high temperature and pressure. Journal of Crystal Growth, 104(2), 578-581.

Arceo, H.B., and Glasser, F.P. (1995) Fluxing reactions of sulfates and carbonates in cement clinkering II. The system $CaCO_3$-K_2CO_3 Cement and Concrete Research, 25(2), 339-344.

Becht, H.Y., and Struikmans, R. (1976) A monoclinic high-temperature modification of potassium carbonate. Acta Crystallographica Section B: Structural Crystallography and Crystal Chemistry, 32(12), 3344-3346.

Brey, G.P., Bulatov, V.K., and Girnis, A.V. (2011) Melting of K-rich carbonated peridotite at 6-10 GPa and the stability of K-phases in the upper mantle. Chemical Geology, 281(3-4), 333-342.

Buob, A., Luth, R.W., Schmidt, M.W., and Ulmer, P. (2006) Experiments on $CaCO_3$-$MgCO_3$ solid solutions at high pressure and temperature. American Mineralogist, 91(2-3), 435-440.

Cancarevic, Z., Schon, J.C., and Jansen, M. (2006) Alkali metal carbonates at high pressure. Zeitschrift Fur Anorganische Und Allgemeine Chemie, 632(8-9), 1437-1448.

Chattaraj, B.D., Dutta, S.N., and Iyengar, M.S. (1973) Studies on the thermal decomposition of calcium carbonate in the presence of alkali salts (Na_2CO_3, K_2CO_3 and NaCl). Journal of Thermal Analysis and Calorimetry, 5(1), 43-49.

Cooper, A.F., Gittins, J., and Tuttle, O.F. (1975) The system Na_2CO_3-K_2CO_3-$CaCO_3$ at 1 kilobar and its significance in carbonatite petrogenesis. American Journal of Science, 275(5), 534-560.

Dalton, J.A., and Presnall, D.C. (1998) Carbonatitic melts along the solidus of model lherzolite in the system CaO-MgO-Al_2O_3-SiO_2-CO_2 from 3 to 7 GPa. Contributions to Mineralogy and Petrology, 131(2-3), 123-135.

Dasgupta, R., and Hirschmann, M.M. (2007) Effect of variable carbonate concentration on the solidus of mantle peridotite. American Mineralogist, 92(2-3), 370-379.

Dasgupta, R., and Hirschmann, M.M. (2010) The deep carbon cycle and melting in Earth's interior. Earth and Planetary Science Letters, 298(1-2), 1-13.

Dasgupta, R., Hirschmann, M.M., and Withers, A.C. (2004) Deep global cycling of carbon constrained by the solidus of anhydrous, carbonated eclogite under upper mantle conditions. Earth and Planetary Science Letters, 227(1-2), 73-85.

Deshpande, D.A., Ghormare, K.R., Deshpande, N.D., and Tankhiwale, A.V. (1993) Dehydration of crystalline $K_2CO_3 \cdot 1.5\ H_2O$. Thermochimica Acta, 66(1-3), 255-265.

Dinnebier, R.E., Vensky, S., Jansen, M., and Hanson, J.C. (2005) Crystal structures and topological aspects of the high-temperature phases and decomposition products of the alkali-metal oxalates M-2[C2O4] (M = K, Rb, Cs). Chemistry-a European Journal, 11(4), 1119-1129.

Dobretsov, N.L., and Shatskiy, A.F. (2012) Deep carbon cycle and geodynamics: the role of the core and carbonatite melts in the lower mantle. Russian Geology and Geophysics, 53(11), 1117-1132.

Dobson, D.P., Jones, A.P., Rabe, R., Sekine, T., Kurita, K., Taniguchi, T., Kondo, T., Kato, T., Shimomura, O., and Urakawa, S. (1996) In-situ measurement of

viscosity and density of carbonate melts at high pressure. Earth and Planetary Science Letters, 143, 207-215.

Eggler, D.H. (1975) Peridotite-Carbonate Relations in the System CaO-MgO-SiO_2-CO_2. Carnegie inst Washington Yearbook, 74, 468-474.

Eitel, W., and Skaliks, W. (1929) Some double carbonates of alkali and earth alkali. Zeitschrift Fur Anorganische Und Allgemeine Chemie, 183(3), 263-286.

Frost, D.J., and McCammon, C.A. (2008) The redox state of Earth's mantle. Annual Review of Earth and Planetary Sciences, 36, 389-420.

Genge, M.J., Price, G.D., and Jones, A.P. (1995) Molecular-dynamics simulations of CaCO3 melts to mantle pressures and temperatures - implications for carbonatite magmas. Earth and Planetary Science Letters, 131(3-4), 225-238.

Grassi, D., and Schmidt, M.W. (2011) The melting of carbonated pelites from 70 to 700 km depth. Journal of Petrology, 52(4), 765-789.

Green, D.H., and Wallace, M.E. (1988) Mantle metasomatism by ephemeral carbonatite melts. Nature, 336(6198), 459-462.

Guillot, B., and Sator, N. (2011) Carbon dioxide in silicate melts: A molecular dynamics simulation study. Geochimica Et Cosmochimica Acta, 75(7), 1829-1857.

Haggerty, S.E. (1989) Mantle metasomes and the kinship between carbonatites and kimberlites. In K. Bell, Ed. Carbonatites: Genesis and Evolution, p. 546-560. Unwin Hyman Ltd, London.

Hammouda, T., and Laporte, D. (2000) Ultrafast mantle impregnation by carbonatite melts. Geology, 28(3), 283-285.

Harlow, G.E. (1997) K in clinopyroxene at high pressure and temperature: An experimental study. American Mineralogist, 82(3-4), 259-269.

Harlow, G.E., and Veblen, D.R. (1991) Potassium in clinopyroxene inclusions from diamonds. Science, 251(4994), 652-655.

Hernlund, J., Leinenweber, K., Locke, D., and Tyburczy, J.A. (2006) A numerical model for steady-state temperature distributions in solid-medium high-pressure cell assemblies. American Mineralogist, 91(2-3), 295-305.

Hunter, R.H., and McKenzie, D. (1989) The equilibrium geometry of carbonate melts in rocks of mantle composition. Earth and Planetary Science Letters, 92(3-4), 347-356.

Izraeli, E.S., Harris, J.W., and Navon, O. (2004) Fluid and mineral inclusions in cloudy diamonds from Koffiefontein, South Africa. Geochimica et Cosmochimica Acta, 68, 2561–2575.

Jago, B.C., and Gittins, J. (1991) The role of fluorine in carbonatite magma evolution. Nature, 349(6304), 56-58.

Kanda, H., Akaishi, M., and Yamaoka, S. (1990) Morphology of synthetic diamonds grown from Na_2CO_3 solvent-catalyst. Journal of Crystal Growth, 106(2-3), 471-475.

Kennedy, C.S., and Kennedy, G.C. (1976) The equilibrium boundary between graphite and diamond. Journal of Geophysical Research, 81(14), 2467-2470.

Kerrick, D.M., and Connolly, J.A.D. (2001a) Metamorphic devolatilization of subducted marine sediments and the transport of volatiles into the Earth's mantle. Nature, 411(6835), 293-296.

-. (2001b) Metamorphic devolatilization of subducted oceanic metabasalts: implications for seismicity, arc magmatism and volatile recycling. Earth and Planetary Science Letters, 189(1-2), 19-29.

Keshav, S., and Gudfinnsson, G.H. (2013) Silicate liquid ‐ carbonatite liquid transition along the melting curve of model, vapor ‐ saturated peridotite in the system CaO ‐ MgO ‐ $Al2O_3$ ‐ SiO_2 ‐ CO_2 from 1.1 to 2 GPa. Journal of Geophysical Research: Solid Earth, 118(7), 3341-3353.

Klein-BenDavid, O., Izraeli, E.S., Hauri, E., and Navon, O. (2004) Mantle fluid evolution - a tale of one diamond. Lithos, 77(1-4), 243-253.

Klement, W., and Cohen, L.H. (1975) Solid-solid and solid-liquid transitions in K_2CO_3, Na_2CO_3 and Li_2CO_3: Investigations to ≥ 5 kbar by differential thermal analysis; thermodynamics and structural correlations. Berichte der Bunsengesellschaft für physikalische Chemie, 79(4), 327-334.

Kröger, C., Illner, K.W., and Graeser, W. (1943) Über die Systeme Alkalioxyd CaO-Al_2O_3-SiO_2-CO_2. XI. Die Reaktionsdrucke im System K_2O-CaO-SiO_2-CO_2. Zeitschrift Fur Anorganische Und Allgemeine Chemie, 251(3), 270-284.

Litasov, K.D. (2011) Physicochemical conditions for melting in the Earth's mantle containing a C–O–H fluid (from experimental data). Russian Geology and Geophysics, 52, 475-492.

Litasov, K.D., Safonov, O.G., and Ohtani, E. (2010a) Origin of Cl-bearing silica-rich melt inclusions in diamonds: Experimental evidence for an eclogite connection. Geology, 38(12), 1131-1134.

Litasov, K.D., Sharygin, I.S., Shatskiy, A.F., Ohtani, E., and Pokhilenko, N.P. (2010b) Experimental constraints on the role of chloride in the origin and evolution of kimberlitic magma. Doklady Earth Sciences, 435(2), 1641-1646.

Litasov, K.D., Shatskiy, A., Ohtani, E., and Yaxley, G.M. (2013) The solidus of alkaline carbonatite in the deep mantle. Geology, 41(1), 79-82.

Liu, Q., Tenner, T.J., and Lange, R.A. (2006) Do carbonate liquids become denser than silicate liquids at pressure? Constraints from the fusion curve of K_2CO_3 to 3.2 GPa. Contributions to Mineralogy and Petrology, 153, 55-66.

Lloyd, E.C., Johnson, D.P., and Hutton, U.O. (1963) Dual-wedge high-pressure appaeatus. Unated States Patent, 3,100,912.

Logvinova, A.M., Wirth, R., Tomilenko, A.A., Afanas'ev, V.P., and Sobolev, N.V. (2011) The phase composition of crystal-fluid nanoinclusions in alluvial diamonds in the northeastern Siberian Platform. Russian Geology and Geophysics, 52(11), 1286-1297.

Luth, R.W. (2006) Experimental study of the $CaMgSi_2O_6$-CO_2 system at 3-8 GPa. Contributions to Mineralogy and Petrology, 151(2), 141-157.

Malik, W.U., Gupta, D.R., Masood, I., and Gupta, R.S. (1985) Kinetic study of thermal decomposition of calcium carbonate in the presence of K_2CO_3 and $BaCO_3$. Journal of Materials Science Letters, 4(5), 532-536.

McKenzie, D., Jackson, J., and Priestley, K. (2005) Thermal structure of oceanic and continental lithosphere. Earth and Planetary Science Letters, 233(3-4), 337-349.

McKie, D. (1990) Subsolidus phase relations in the system $K_2Ca(CO_3)_2$-$Na_2Mg(CO_3)_2$ at 1 kbar: The fairchildite$_{ss}$-buetschliite-eitelite eutectoid. American Mineralogist, 75(9-10), 1147-1150.

Minarik, W.G., and Watson, E.B. (1995) Interconnectivity of carbonate melt at low melt fraction. Earth and Planetary Science Letters, 133(3-4), 423-437.

Navon, O. (1991) High internal pressure in diamond fluid inclusions determined by infrared absorption. Nature, 353(6346), 746-748.

Niggli, P. (1916) Gleichgewichte zwischen TiO_2 und CO_2, sowie SiO_2 und CO_2 in Alkali-, Kalk-Alkali und Alkali-Aluminatschmelzen. Zeitschrift Fur Anorganische Und Allgemeine Chemie, 98(1), 241-326.

Osugi, J., Shimizu, K., Inoue, K., and Yasunami, K. (1964) A compact cubic anvil high pressure apparatus. Review of Physical Chemistry of Japan, 34(1), 1-6.

Pal'yanov, Y.N., Sokol, A.G., Borzdov, Y.M., and Khokhryakov, A.F. (2002) Fluid-bearing alkaline carbonate melts as the medium for the formation of diamonds in the Earth's mantle: an experimental study. Lithos, 60(3-4), 145-159.

Pal'yanov, Y.N., Sokol, A.G., Borzdov, Y.M., Khokhryakov, A.F., Gusev, V.A., and Sobolev, N.V. (1997) Growth and characterization of diamond single crystals up to four carats. Doklady Akademii Nauk, 355(6), 798-800.

Pal'yanov, Y.N., Sokol, A.G., Borzdov, Y.M., Khokhryakov, A.F., Shatsky, A.F., and Sobolev, N.V. (1999) The diamond growth from Li_2CO_3, Na_2CO_3, K_2CO_3 and Cs_2CO_3 solvent-catalysts at P=7 GPa and T=1700-1750 ^{o}C. Diamond and Related Materials, 8(6), 1118-1124.

Pal'yanov, Y.N., Sokol, A.G., Borzdov, Y.M., Khokhryakov, A.F., and Sobolev, N.V. (1998) Crystallization of diamond in the $CaCO_3$-C, $MgCO_3$-C and $CaMg(CO_3)_2$-C systems. Doklady Akademii Nauk, 363(2), 230-233.

Palyanov, Y.N., Bataleva, Y.V., Sokol, A.G., Borzdov, Y.M., Kupriyanov, I.N., Reutsky, V.N., and Sobolev, N.V. (2013) Mantle–slab interaction and redox mechanism of diamond formation. Proceedings of the National Academy of Sciences, 110(51), 20408-20413.

Palyanov, Y.N., Borzdov, Y.M., Khokhryakov, A.F., Kupriyanov, I.N., and Sokol, A.G. (2010) Effect of nitrogen impurity on diamond crystal growth processes. Crystal Growth & Design, 10(7), 3169-3175.

Palyanov, Y.N., and Sokol, A.G. (2009) The effect of composition of mantle fluids/melts on diamond formation processes. Lithos, 112, 690-700.

Pollack, H.N., and Chapman, D.S. (1977) On the regional variation of heat flow, geotherms, and lithospheric thickness. Tectonophysics, 38, 279-296.

Ragone, S.E., Datta, R.K., Roy, D.M., and Tuttle, O.F. (1966) The System Potassium Carbonate-Magnesium Carbonate. Journal of Physical Chemistry, 70(10), 3360-3361.

Rohrbach, A., Ballhaus, C., Golla-Schindler, U., Ulmer, P., Kamenetsky, V.S., and Kuzmin, D.V. (2007) Metal saturation in the upper mantle. Nature, 449(7161), 456-458.

Schneide, S.J., and Levin, E.M. (1973) Polymorphism of K_2CO_3. Journal of the American Ceramic Society, 56(4), 218-219.

Schrauder, M., and Navon, O. (1994) Hydrous and carbonatitic mantle fluids in fibrous diamonds from Jwaneng, Botswana. Geochimica Et Cosmochimica Acta, 58(2), 761-771.

Sharygin, I.S., Litasov, K.D., Shatskiy, A.F., Golovin, A.V., Ohtani, E., and Pokhilenko, N.P. (2013) Melting of kimberlite of the Udachnaya East pipe: experimental study at 3–6.5 GPa and 900–1500°C. Doklady Earth Sciences, 448, 200-205.

Shatskii, A.F., Borzdov, Y.M., Sokol, A.G., and Pal'yanov, Y.N. (2002) Phase formation and diamond crystallization in carbon-bearing ultrapotassic carbonate-silicate systems. Geologiya I Geofizika, 43(10), 940-950.

Shatskiy, A., Borzdov, Y.M., Litasov, K.D., Kupriyanov, I.N., Ohtani, E., and Palyanov, Y.N. (2014) Phase relations in the system $FeCO_3$-$CaCO_3$ at 6 GPa

and 900-1700 °C and its relation to the system $CaCO_3$-$FeCO_3$-$MgCO_3$. American Mineralogist, 99(4), 773-785.

Shatskiy, A., Borzdov, Y.M., Litasov, K.D., Ohtani, E., Khokhryakov, A.F., Pal'yanov, Y.N., and Katsura, T. (2011a) Pressless split-sphere apparatus equipped with scaled-up Kawai-cell for mineralogical studies at 10–20 GPa. American Mineralogist, 96(4), 541-548.

Shatskiy, A., Gavryushkin, P.N., Sharygin, I.S., Litasov, K.D., Kupriyanov, I.N., Higo, Y., Borzdov, Y.M., Funakoshi, K., Palyanov, Y.N., and Ohtani, E. (2013a) Melting and subsolidus phase relations in the system Na_2CO_3-$MgCO_3$+-H_2O at 6 GPa and the stability of $Na_2Mg(CO_3)_2$ in the upper mantle. American Mineralogist, 98(11-12), 2172-2182.

Shatskiy, A., Katsura, T., Litasov, K.D., Shcherbakova, A.V., Borzdov, Y.M., Yamazaki, D., Yoneda, A., Ohtani, E., and Ito, E. (2011b) High pressure generation using scaled-up Kawai-cell. Physics of the Earth and Planetary Interiors, 189(1-2), 92-108.

Shatskiy, A., Litasov, K.D., Borzdov, Y.M., Katsura, T., Yamazaki, D., and Ohtani, E. (2013b) Silicate diffusion in alkali-carbonatite and hydrous melts at 16.5 and 24 GPa: Implication for the melt transport by dissolution-precipitation in the transition zone and uppermost lower mantle. Physics of the Earth and Planetary Interiors, 225, 1-11.

Shatskiy, A., Litasov, K.D., Matsuzaki, T., Shinoda, K., Yamazaki, D., Yoneda, A., Ito, E., and Katsura, T. (2009) Single crystal growth of wadsleyite. American Mineralogist, 94(8-9), 1130-1136.

Shatskiy, A., Sharygin, I.S., Gavryushkin, P.N., Litasov, K.D., Borzdov, Y.M., Shcherbakova, A.V., Higo, Y., Funakoshi, K., Palyanov, Y.N., and Ohtani, E. (2013c) The system K_2CO_3-$MgCO_3$ at 6 GPa and 900-1450 ºC. American Mineralogist, 98(8-9), 1593-1603.

Shatskiy, A., Sharygin, I.S., Litasov, K.D., Borzdov, Y.M., Palyanov, Y.N., and Ohtani, E. (2013d) New experimental data on phase relations for the system Na_2CO_3-$CaCO_3$ at 6 GPa and 900-1400 ºC. American Mineralogist, 98(11-12), 2164-2171.

Shatskiy, A., Yamazaki, D., Borzdov, Y.M., Matsuzaki, T., Litasov, K.D., Cooray, T., Ferot, A., Ito, E., and Katsura, T. (2010) Stishovite single-crystal growth and application to silicon self-diffusion measurements. American Mineralogist, 95(1), 135-143.

Shatsky, V.S., Sobolev, N.V., and Vavilov, M.A. (1995) Diamond-bearing metamorphic rocks from the Kokchetav massif (Northern Kazakhstan). In R.G. Coleman, and X. Wang, Eds. Ultrahigh Pressure Metamorphism, p. 427-455. Cambridge University Press.

Sobolev, N.V., Bakumenko, I.T., Yefimova, E.S., and Pokhilenko, N.P. (1991) Peculiarities of microdiamond morphology, sodium content in garnets and potassium content in pyroxenes of 2 eclogite xenoliths from the Udachnaya kimberlite pipe (Yakutia). Doklady Akademii Nauk Sssr, 321(3), 585-592.

Sobolev, N.V., and Shatsky, V.S. (1990) Diamond inclusions in garnets from metamorphic rocks: a new environment for diamond formation. Nature, 343(6260), 742-746.

Sobolev, V.S., Sobolev, N.V., and Lavrent'yev, Y.G. (1972) Inclusions in diamond from diamondiferous eclogite. Doklady Akademii Nauk SSSR, 207, 164-167.

Sokol, A.G., Palyanov, Y.N., and Surovtsev, N.V. (2007) Incongruent melting of gallium nitride at 7.5 GPa. Diamond and Related Materials, 16(3), 431-434.

675 Sokol, A.G., Tomilenko, A.A., Pal'yanov, Y.N., Borzdov, Y.M., Pal'yanova, G.A.,
676 and Khokhryakov, A.F. (2000) Fluid regime of diamond crystallisation in
677 carbonate-carbon systems. European Journal of Mineralogy, 12(2), 367-375.
678 Suito, K., Namba, J., Horikawa, T., Taniguchi, Y., Sakurai, N., Kobayashi, M.,
679 Onodera, A., Shimomura, O., and Kikegawa, T. (2001) Phase relations of
680 $CaCO_3$ at high pressure and high temperature. American Mineralogist, 86(9),
681 997-1002.
682 Sweeney, R.J. (1994) Carbonatite melt compositions in the Earth's mantle. Earth and
683 Planetary Science Letters, 128(3-4), 259-270.
684 Tomlinson, E.L., Jones, A.P., and Harris, J.W. (2006) Co-existing fluid and silicate
685 inclusions in mantle diamond. Earth and Planetary Science Letters, 250(3-4),
686 581-595.
687 Wallace, M.E., and Green, D.H. (1988) An experimental determination of primary
688 carbonatite magma composition. Nature, 335(6188), 343-346.
689 Weiss, Y., Kessel, R., Griffin, W.L., Kiflawi, I., Klein-BenDavid, O., Bell, D.R.,
690 Harris, J.W., and Navon, O. (2009) A new model for the evolution of
691 diamond-forming fluids: Evidence from microinclusion-bearing diamonds
692 from Kankan, Guinea. Lithos, 112(S2), 660-674.
693 Wyllie, P.J., and Huang, W. (1975) Peridotite, kimberlite, and carbonatite explained
694 in the system CaO-MgO-SiO_2-CO. Geology, 3, 621-624.
695 Yaxley, G.M., and Brey, G.P. (2004) Phase relations of carbonate-bearing eclogite
696 assemblages from 2.5 to 5.5 GPa: implications for petrogenesis of carbonatites.
697 Contributions to Mineralogy and Petrology, 146(5), 606-619.
698 Yoshino, T., Laumonier, M., McIsaac, E., and Katsura, T. (2010) Electrical
699 conductivity of basaltic and carbonatite melt-bearing peridotites at high
700 pressures: Implications for melt distribution and melt fraction in the upper
701 mantle. Earth and Planetary Science Letters, 295(3-4), 593-602.
702 Zedgenizov, D.A., Ragozin, A.L., Shatsky, V.S., Araujo, D., and Griffin, W.L. (2011)
703 Fibrous diamonds from the placers of the northeastern Siberian Platform:
704 carbonate and silicate crystallization media. Russian Geology and Geophysics,
705 52(11), 1298-1309.
706 Zedgenizov, D.A., Ragozin, A.L., Shatsky, V.S., Araujo, D., Griffin, W.L., and Kagi,
707 H. (2009) Mg and Fe-rich carbonate-silicate high-density fluids in cuboid
708 diamonds from the Internationalnaya kimberlite pipe (Yakutia). Lithos,
709 112(S2), 638-647.
710